Colloids and Surfaces B: Biointerfaces 121 (2014) 281–289

Contents lists available at ScienceDirect

Colloids and Surfaces B: Biointerfaces

journal homepage: www.elsevier.com/locate/colsurfb

Structural features of ultradeformable archaeosomes for topical delivery of ovalbumin

Dolores C. Carrer[b], Leticia H. Higa[a], Maria Victoria Defain Tesoriero[a,c], Maria Jose Morilla[a], Diana I. Roncaglia[a], Eder Lilia Romero[a,*]

[a] Programa de Nanomedicinas, Departamento de Ciencia y Tecnología, Universidad Nacional de Quilmes, Roque Saenz Peña 352, Bernal, B1876 BXD Buenos Aires, Argentina
[b] Instituto Ferreyra, INIMEC-CONICET, casilla de correo 389, 5000 Cordoba, Argentina
[c] Unidad Operativa Sistemas de Liberación Controlada, Centro de Investigación y Desarrollo en Química, Instituto Nacional de Tecnología Industrial (INTI), Av. General Paz 5445, B1650WAB Buenos Aires, Argentina

ARTICLE INFO

Article history:
Received 31 January 2014
Received in revised form 3 May 2014
Accepted 9 May 2014
Available online 22 May 2014

Keywords:
Ultradeformable archaeosomes
Skin
Penetration

ABSTRACT

The ultradeformable archaeosomes (UDA, made of total polar archaeolipids (TPA) extracted from the extreme halophile archaea *Halorubrum tebenquichense*:soybean phosphatidylcholine (SPC):sodium cholate (NaChol), 3:3:1 w:w), are promising topical adjuvants showing high deformability, an essential property for intact skin penetration up to the viable epidermis/dermis. To gain insights on UDA structure, the interactions between TPA, SPC and the edge activator NaChol, were assessed by electrospray ionization mass spectroscopy (ESI-MS) and confocal fluorescence microscopy of giant unilamellar vesicles (GUV). The non covalent heterodimers NaChol–SPC, NaChol–phosphatidylglycerophosphate methyl ether (PGPMe), NaChol–sulfated diglycosyl diphytanyl–glycerol diether (SDGD5) and SPC–PGPMe detected in the gas phase by ESI-MS after direct infusion of UDA, together with the homogeneous partition of FASTDiO and DiIC18 in GUV suggested that in these proportions, lipids and NaChol were miscible. We propose therefore, a model where in UDA the SPC diluted sufficient enough in the rich PGPMe TPA, so as to the low lateral mobility of molecules (typical of rich in PGPMe bilayers) was no longer experienced. We also found that 50 μm deep within *in vitro* human skin canyons, the fluorescence of Alexa fluor 647-ovalbumin in UDL was ~1.5 folds higher than in UDA, indicating a potential steric hindrance of the voluminous structure of PGPMe UDA bilayer, to the penetration of a particulate cargo such as the 7 nm diameter ovalbumin. According to these observations, a further reduction in PGPMe – a lipid playing no immune role – content could help to improve the performance of UDA as topical adjuvants.

1. Introduction

The ultradeformable liposomes (UDL) are liposomes prepared with phospholipids plus a certain proportion of edge activators (EA), usually detergents such as sodium cholate, Tween 80 or Spam 80. Their structural development and mechanical properties were first described by Cevc in 1992 [1]. Applied on the skin surface under non occlusive conditions, the lipid bilayer of UDL efficiently penetrates the outermost layer of the skin, the stratum corneum (SC), carrying small molecules up to the viable epidermis nearly tens of micrometers depth [2,3]. Besides of being used as drug delivery systems, there is a growing interest on their application as adjuvants for topical vaccination to elicit antigen-dependent and memory systemic and mucosal responses [4–6]. The topical vaccination is strategic for developing countries because of the avoidance of injectables, need for a cold chain, use of sterile material and trained personal for administration. The ultradeformable archaeosomes (UDA) are a variety of UDL containing Total Polar Archaeolipids (TPA) extracted from the extreme halophile archaea *Halorubrum tebenquichense*. The TPA are a mixture of sn2,3 glycerol ethers with polyisoprenoid chains, some of them bearing sugar polar headgroups. Their ether linkages instead of ester and stereoisomery different from sn 1,2,... are chemical characteristics that provide resistance to the hydrolysis and oxidation in comparison to classical phospholipid bilayers [7]. The classical work of Sprott showed that archaeosomes (ARC) (fully made of TPA liposomes) induce a strong systemic antigen-dependent and memory response when subcutaneously injected in mice [8]. We

* Corresponding author. Tel.: +54 1143657100; fax: +54 1143657132.
E-mail addresses: elromero@unq.edu.ar, eder19lilia@gmail.com (E.L. Romero).

http://dx.doi.org/10.1016/j.colsurfb.2014.05.015
0927-7765/

have recently shown that UDA made of TPA:soybean phosphatidylcholine (SPC):sodium cholate (NaChol) (3:3:1 w:w) are more avidly taken up by macrophages (J774 cells) than UDL and generate an ovalbumin-dependent systemic immune response of higher intensity than UDL, when topically applied on Balb/c mice [9]. In this work, with the aim of explaining the need for adding SPC to TPA:NaChol mixtures in order to make bilayers highly deformable, a direct infusion electrospray ionization mass spectrometry (ESI-MS) approach was used to reveal the existence of non covalent intermolecular associations between the UDA components. To gain insights on the structural features of UDA, the spectrometric data was complemented with confocal fluorescence microscopy images of giant unilamellar vesicles (GUV) made of TPA, SPC and NaChol and with an *in vitro* assay where the usefulness of UDA to deliver the model macromolecule ovalbumin to canyons and cell clusters of the viable epidermis was compared to that of UDL, conventional liposomes and ARC.

2. Materials and methods

2.1. Materials

Soybean phosphatidylcholine (SPC) (phospholipon 90 G, purity >90%) was a gift from Phospholipid/Natterman, Germany. Sodium cholate (NaChol), Sephadex G-75 and ovalbumin fluorescently labeled with Alexa fluor 647 (Alexa 647-OVA) were from Sigma-Aldrich, Argentina. The fluorescent probes FASTDiO (3,3′-dilinoleyloxacarbocyanine perchlorate, DiO$\Delta^{9,12}$-C_{18}(3), ClO_4) and DiIC18 (1,1′-dioctadecyl-3,3,3′,3′-tetramethylindocarbocyanine perchlorate) were from molecular probes (Eugene, OR, USA). All other chemicals and reagents were of analytical grade from Anedra, Argentina.

2.2. Archaebacteria growth, extraction and characterization of total polar lipids

Halorubrum tebenquichense archaeas, isolated from soil samples of Salina Chica, Península de Valdés, Chubut, Argentina [10], was grown in 8 L batch cultures in basal medium supplemented with yeast extract and glucose. Cultures were monitored by absorbance at 660 nm and harvested in late stationary phase for storage as frozen cell pastes.

Total lipids were extracted from frozen and thawed biomass using the Bligh and Dyer method as modified for extreme halophiles and the Total Polar Archaeolipid (TPA) fraction was collected by precipitation from cold acetone [11]. Between 90 and 120 mg TPA were isolated from each culture batch. The reproducibility of each TPA extract's composition was routinely screened by phosphate content [12], and electrospray ionization mass spectrometry (ESI-MS). For negative ion ESI-MS, TPA extracts were dissolved in chloroform: methanol (1:1; vol/vol) and injected in a Thermo Finnigan LCQ Ion Max mass spectrometer (Thermo Finnigan MAT, San Jose, CA, USA) equipped with a electrospray ionization source, interface conditions were: nebulizer gas (air) 12 μL/min, curtain gas (nitrogen) 1.2 μL/min, needle voltage −4 kV.

2.3. Preparation of nanoliposomes

Ultradeformable archeosomes (UDA, made of TPA:SPC:NaChol, 3:3:1 w:w), ternary bilayers liposomes (TPA:SPC:NaChol, 4:2:1 and 2:4:1, w:w), binary bilayers liposomes (made of TPA:NaChol, 6:1 w:w), archaeosomes (ARC, fully made of TPA), ultradeformable liposomes (UDL, made of SPC:NaChol, 6:1 w:w) and conventional liposomes (L, fully made of SPC) were prepared by the thin film hydratation method. Briefly, appropriate amounts of SPC in chloroform and TPA and NaChol in chloroform:methanol (1:1, v:v) were mixed in round bottom flasks. Solvents were rotary evaporated at 40 °C until elimination and the lipid films obtained were flushed with N_2. Lipid films were hydrated by the addition of an aqueous phase (10 mM Tris–HCl buffer plus 0.9% w/v NaCl, pH 7.5 (Tris–HCl buffer)) up to a final concentration of 43 mg of phospholipids/mL. The resultant suspensions were sonicated (45 min with a bath type sonicator 80 W, 40 kHz) and extruded 15 times through three stacked 0.2, 0.1 and 0.1 μm pore size polycarbonate filters using a 100 mL Thermobarrel extruder (Northern Lipids, Canada).

To prepare Alexa 647-OVA loaded nanoliposomes (OVA-UDA, OVA-UDL, OVA-L and OVA-ARC), Alexa 647-OVA was dissolved in the aqueous phase used for the hydration of the thin film at 1.15 mg/mL. After extrusion, nanoliposomes were submitted to five freeze–thaw cycles between −70 °C and 40 °C. Finally, vesicles were purified on Sephadex G-75 using the minicolumn centrifugation technique [13]. The OVA/phospholipid ratio was determined by protein [14] and phospholipid quantification.

2.4. Characterization of nanoliposomes

Phospholipids were quantified as stated above. Size and zeta potential of nanoliposomes were determined by dynamic light scattering (DLS) and phase analysis light scattering (PALS), respectively, using a nanoZsizer apparatus (Malvern Instruments, UK).

2.5. Measurement of deformability

The deformability value (D) of the nanoliposomes was calculated according to Van den Bergh et al. [15] as $D = J(rv/rp)^2$, where J is the rate of penetration through a permeability barrier, rv is the post extrusion liposomal radii and rp is the extrusion membrane pore radii. To measure J, nanoliposomes were extruded through two stacked 50 nm rp membranes at 0.8 MPa using a Thermobarrel extruder. Extruded volume was collected every minute along 15 min, phospholipid was quantified in each fraction and J was calculated as the area under the curve of the plot of phospholipid recovered as a function of time. The average post extrusion liposomal radii (rv) was measured by DLS.

2.6. Electrospray ionization mass spectrometry of lipids and nanoliposomes

The following samples were directly infused by ESI-MS in positive (at 4 kV capillary exit voltage) or negative modes as stated above: UDL and UDA in aqueous buffer, TPA:SPC in $CHCl_3$:CH_3OH (1:1 v/v), SPC:NaChol in $CHCl_3$:CH_3OH (1:1 v/v). The running conditions were the same as in 2.2 excepting the needle capillary exit voltage, which was varied between 3, 3.5 and 4 kV.

2.7. Giant unilamellar vesicles production and imaging

Giant unilamellar vesicles (GUVs) were prepared by the electroformation procedure [16]. In brief, the lipids dissolved in organic solvent were mixed in the desired proportions at a concentration of 10 mg/mL. Fluorescent lipid analogs were added to the mixture at a lipid:fluorescent probe proportion of 100:0.2. The lipid solution was then applied to the Pt wires of a home-made Teflon chamber [17] and let at 60 °C for 10 min to evaporate the solvent. The electroformation was then performed in a 300 mOsM sucrose solution at 40 °C for 3 h. The GUVs thus formed were gently transferred to an observation chamber filled with 300 mOsM glucose and taken to the microscope, where they were imaged at room temperature.

The vesicles were imaged in a Zeiss Pascal laser scanning confocal microscope. The objective used was a Plan-Apochromat 63 × 1.4 n.a. Oil DIC. FASTDiO was excited with the 488 nm line of an Argon

laser. The emission light was collected through a 505–530 bandpass filter. DiI was excited with the 543 nm line of an He–Ne laser. The emission light was collected through a long pass 560 filter.

2.8. Quantification of in vitro skin penetration of Alexa 647-OVA-labeled nanovesicles

Abdominal human skin was obtained from anonymous cosmetic surgery patients. The ages of the patients ranged between 35 and 45 years old and were all female. The skin samples were immediately frozen at −20 °C after the surgery and used within six weeks [18]. Skin samples of approx. 1 cm^2 area were incubated for 2 h at 35 °C with 16 μL of nanoliposomes suspensions at 750 μg lipids/cm^2 (or the corresponding amount of free Alexa 647-OVA in buffer), distributed as small droplets of 2 μL each all over the surface. The samples were afterwards fixed with paraformaldehide 5% for 3 h. Data shown were the mean of at least five samples from each patient.

Confocal fluorescence microscopy was performed in a Zeiss 710 microscope. The objective used was a W-Plan Apochromat 20×/1.0 DIC M27 70 mm. We used the 633 nm line of an He–Ne laser to excite Alexa647 and a 405 diode laser to excite autofluorescence. The emission of Alexa 647 was collected through a 644–740 nm bandpass filter. The autofluorescence emission was collected through a 420–480 nm bandpass filter.

The fluorescence intensity in different regions was quantified by the ImageJ software. The area to be quantified in each image was manually chosen, a histogram of pixel intensities distribution was obtained and the mean was taken. These values were then normalized by the amount of area analyzed on each image. The laser intensity was varied as the laser focus got deeper into the skin, since scattering by the tissue would otherwise make it impossible to measure after the first few microns in the skin. All data shown in this section were thus corrected.

3. Results and discussion

In this work the structural features of UDA, nanoliposomes that combine a specific mechanical property such as high deformability, with high uptake by macrophages were assessed by mechanical (flow across a nanoporous barrier) spectroscopic (ESI-MS) and confocal fluorescence microscopy of GUV techniques.

3.1. Deformability of nanoliposomes

The structural characteristics of nanoliposomes are shown in Table 1. The Van der Bergh assay is a simple method used to identify highly deformable nanoliposomes. In there the nanoliposomal flux under a low extrusion pressure across membranes of pore radii half of the liposomal radii (usually 100 nm mean diameter) and the mean size post-extrusion are measured. As a result, the relative deformability (D) –which is inversely proportional to the absolute elastomechanic parameter Young's modulus – is determined. Hence, non-deformable nanoliposomes (L) of 1119 ± 242 kiloPascals (kPa) Young's modulus (as measured by atomic force microscopy [19]) or 1970 ± 750 kPa according to Guangzhao et al. [20], were difficultly extruded, rendered a low flux and a decreased post-extrusion size, resulting in a D of 765 ± 120. TPA:NaChol (6:1 w:w) and TPA:SPC:NaChol (4:2:1 w:w) nanoliposomes of D similar to L, were therefore classified as non-deformable. Since it was not possible to extrude ARC, these nanoliposomes were classified as non-deformable as well. Instead, UDL of much lower Young's modulus (430 ± 137 kPa) [19] had a considerably higher D than L. The TPA:SPC:NaChol (3:3:1 w:w) of 294 ± 177 kPa Young's modulus [19] and TPA:SPC:NaChol (2:4:1 w:w) (1/2 and 2/3 parts of TPA were replaced by SPC) nanoliposomes on the other hand, of D similar to UDL were also classified as highly deformable.

For NaChol to decrease the Young's modulus of SPC bilayers acting as edge activator, it has to partition within SPC, and respond with a mixing/demixing to the mechanical stress of deformation [21]. When UDL are submitted to a local stress of deformation, such as elongation or lost of sphericity, the individual components, initially homogeneously mixed, are partly separated in the bilayer (demixing). The most soluble ingredients (NaChol) are accumulated within the sites of highest curvature, while those less soluble (phospholipids) become more abundant on the zones of lower deformation. The demixing of components alleviates the highly curved zones and allows the reversible local protrusion in these sites [22]. However, as we previously reported [9], the addition of NaChol to TPA did not produce highly deformable nanoliposomes. In other words NaChol did not act as an edge activator as occurred in UDL. We failed in attempting to increase its D by incrementing the NaChol content, since at 1 mg NaChol per 6 mg phospholipids ratio, in 43 mg phospholipids/mL the NaChol concentration is close to its critical micellar concentration (cmc) [23]. However, we observed that if TPA was replaced by a given amount of SPC, the D could be increased. In particular, we observed here that TPA had to be replaced by a minimal amount of SPC starting from 1/2 in weight of TPA (corresponding to 3:3:1 w:w), since by replacing 1/3 of TPA (corresponding to 4:2:1 w:w) the nanoliposomes were non-deformable, while by replacing 2/3 of TPA (corresponding to 2:4:1 w:w) the nanoliposomes were highly deformable. Moreover, by reaching this minimal (3:3:1 w:w) SPC threshold, the D of TPA:SPC:NaChol nanoliposomes increased up to the value of high deformability, but a further increment of SPC however, had no effect on D.

According to Cevc [24], the lateral displacement of NaChol in the bilayer is responsible for the high D of UDL. We speculate that the low D of TPA:NaChol (6:1 w:w) and of TPA:SPC:NaChol (4:2:1 w:w) nanoliposomes could be owed to two alternative reasons: (a) a dynamic one, because of an absent/difficult lateral displacement of NaChol in TPA or TPA:SPC (absent mixing/demixing), or (b) because of the absent NaChol partition in TPA or TPA:SPC. In the first case, in spite of partitioning in the bilayer, the lateral displacement of NaChol is impaired; nonetheless, non covalent association between NaChol and TPA has to be present; in the second case, the absent partition would be reflected in the absence of non covalent association. From this point of view, by revealing the non covalent associations between NaChol and bilayer lipids could help to understand the source of the impaired D on TPA containing bilayers. To meet that aim, we analyzed by direct infusion ESI-MS technique UDL and UDA in aqueous buffer as well as SPC:NaChol, TPA:NaChol and TPA:SPC mixtures in organic solvent.

3.2. ESI-MS to detect non covalent interactions between lipids and sodium cholate

The ESI-MS technique is an extremely soft method for molecular ionization in the gaseous phase, which induces the formation of molecular ions (protonated, deprotonated species, and adducts) [25]. In the field of lipidomics, ESI-MS has proven useful in lipids identification and quantification [26]. Elaborated studies based on this technique has been applied to quantify different types of non covalent associations such as electrostatic interactions (*e.g.*, salt bridges), dipolar interactions (*e.g.*, hydrogen bonds), and van der Waals interactions (*e.g.*, hydrophobic interactions) [27], between protein–protein, protein–small molecule, and protein–DNA complexes [28,29].

A well known feature of this technique is that the hydrophobic effect is mostly lost once the molecular ions desolvate to enter the gas phase [30]. Because of this, supramolecular aggregates with a

Table 1
Structural characteristics of the liposomes.

Composition (w:w)	*Z* potential* (mV)	Mean size (nm)* (polydispersity index)	Mean size (nm) post extrusion	*D*
SPC (L)	−10 ± 3	109 ± 5 (0.103)	62 ± 6	765 ± 120
TPA (ARC)	−34 ± 2	190 ± 20 (0.305)	–	*e.n.p.*
SPC:NaChol (6:1) (UDL)	−12 ± 2	110 ± 2 (0.242)	109 ± 2	3882 ± 200
TPA:NaChol (6:1)	−33 ± 2	673 (80%) 60 (20%)[a] (0.781)	84 ± 3	1057 ± 210
TPA:SPC:NaChol (4:2:1)	−36.6 ± 1	128 ± 1 (0.255)	112 ± 0.6	1321 ± 125
TPA:SPC:NaChol (3:3:1) (UDA)	−35 ± 4	130 ± 1 (0.241)	110 ± 2	4064 ± 140
TPA:SPC:NaChol (2:4:1)	−36.6 ± 1	128 ± 1 (0.255)	115 ± 5	3890 ± 130

* Values represent mean ± SD ($n = 3$).
[a] Two populations were present; *e.n.p.:* extrusion was not possible.

structure depending on the hydrophobic effect, as well as the native structure of globular and membrane proteins, are not expected to be retained in an ESI-MS spectra [31,32]. Nonetheless, the aggregation number and cmc of micelles of different surfactants can be determined after being *directly infused* in aqueous buffer. Remarkably, the aggregation number of micelles stabilized by ionic and polar (such as hydrogen bonding) non covalent bonds, the ones that remain and become prominent in the gas phase, are the only that can be observed [29,33].

Liposomes are out of the thermodynamic equilibrium closed bilayers, of much higher size and aggregation number than micelles [34]. But similar to micelles, the hydrophobic effect is the main responsible for the maintenance of the liposomal supramolecular architecture. Because of this, after desolvation and gas phase entrance, the supramolecular structure of liposomes is expected to be destabilized/disordered [35]. However, the same as for micelles, some bilayer components could remain associated as long as their interaction is mediated by the non covalent interactions before mentioned. These interactions are for instance responsible, for partitioning or dynamic miscibility between lipids and or detergents within liposomal bilayers, such as those between phosphatidylcholine and NaChol, that at 6:1 w:w result in highly deformable bilayers [36]. Such interaction in liposomal bilayers suggests that, at these proportions, the components form homogeneous phases; in other words, reflects their miscibility.

In liposomes bilayers, immiscible phospholipids (usually grouped on the bases of their capacity to form ordered or disordered arrangements when differing in more than four carbon units) are packed in domains separated by phase boundaries [37]. We had previously observed the absence of heterodimers after direct infusion in ESI-MS of 100 nm sized nanoliposomes made of components coexisting as disordered:ordered domains in bilayers, such as dilaurylphosphatidylcholine (DLPC)–distearoyl phoshatidylcholine (DSPC) (1:1 w:w) at 25 °C, [38] and others (data not shown). Here, the non covalent interactions after direct infusion of UDL and UDA in aqueous buffer both in positive and negative mode revealed the signals listed in Table 2. At 3 kV, although the main peaks and the signals noise had reduced intensities, the less intense signals of the non covalent interactions were optimally detected. However, by increasing the cone voltage to 3.5 and 4 kV, did not allow distinguishing between the different strengths of the non covalent interactions.

As expected, in Fig. 1a the signal of SPC appeared after direct infusion of UDL in positive mode; the SPC–SPC homodimers and NaChol–Na+ adducts on the other hand reflected the association trend of these amphiphilic molecules (Table 2). Besides, the SPC–NaChol heterodimers revealed the *in situ* partition of NaChol within SPC in SPC:NaChol (6:1 w:w) bilayers. The signals of NaChol and its homodimer appeared after direct infusion of UDL negative mode (Fig. 1Sa). Identical signals to those in Fig. 1a appeared after direct infusion of SPC:NaChol (6:1 w:w) mixture in organic solvent (Fig. 1Sb), suggesting the hydrophobic effect was not underlying these non covalent associations.

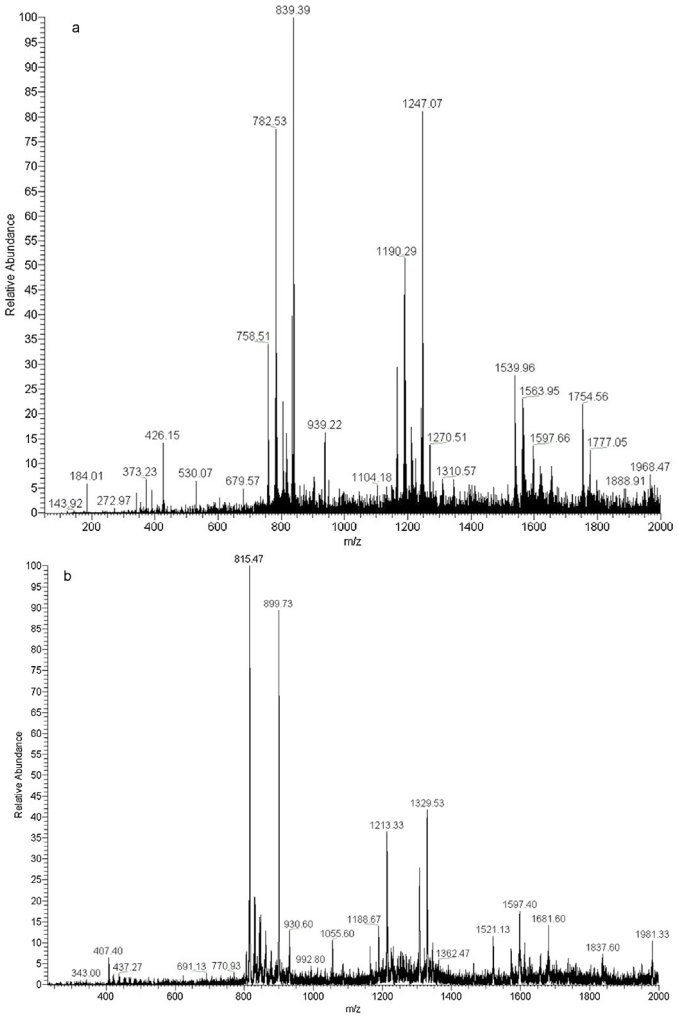

Fig. 1. Direct infusion ESI-MS spectra of UDL, positive mode (a) and UDA, negative mode (b).

On the other hand, the signal of phosphatidylglycerophosphate methyl ether PGPMe (highly abundant in TPA from extreme halophile archaeas), sulfated diglycosyl diphytanyl–glycerol diether (SDGD5), bisphosphatidylglycerol (BPG) and NaChol appeared after direct infusion of UDA in negative mode, as well as the NaChol–NaChol homodimers (Fig. 1b). The PGPMe–PGPMe homodimer was not identified (probably because of its signal at 1798 is close to the detection limit of the equipment at 2000 amu; alternatively, the low inter PGPMe interactions could be another reason as discussed below); other potential intra TPA non covalent interactions, if existing, were not detected if lied beyond 200 amu. Nonetheless, the most relevant findings were

Table 2
ESI-MS spectra assignments.

Sample	Identified species (observed *m/z*)			
UDL (+)	SPC 758 PC (16:0/18:2) 782 PCSPC–SPC 1540 (18:2/18:2) [780 = 758 + 22] [758 + 782] 804 PC (782 + Na^+) 1563 [758 + 804]	SPC–NaChol 1190 [782 + 407]	NaChol–NaChol 839 [dimer + Na^+] 1247 [trimer + Na^+]	
UDL (−)	NaChol 407	NaChol–NaChol 815 [Dimmer]		
SPC:NaChol (+)	SPC 758 782 804	SPC–SPC 1540 [758 + 782] 1563 [782 + 407] [758 + 804]	SPC–NaChol 1190	NaChol–NaChol 839
UDA (−)	TPA 899 PGPMe 1056 S-DGD5 1521 BPG	NaChol 407	SPC–NaChol 1189	NaChol–NaChol 815 [dimer]
UDA (+)	SPC–SPC 1539			
TPA:NaChol (−)	TPA 899 PGPMe 1056 S-DGD5 1521 BPG	NaChol 407	NaChol–NaChol 815 1221 [Trimer]	
TPA:SPC (−)	TPA 899 PGPMe 1056 S-DGD5 1521 BPG		PGPMe–SPC 1657 [899 + 758] 1681 [899 + 782] 1703 [899 + 804]	
TPA:SPC (+)	SPC–SPC 1540 1564			

PGPMe–SPC 1681 [899 + 782]	PGPMe–NaChol 1307 [899+407]	S-DGD5-NaChol 1463 [1056+407]	
PGPMe–NaChol 1307			

the SPC–PGPMe, SPC–NaChol PGPMe–NaChol and SDGD5–NaChol heterodimers. The existence of non covalent interactions between SPC and TPA suggested their miscibility, and potential existence of homogeneous phases. Accordingly, the NaChol–SPC and NaChol–PGPMe interactions would indicate that in UDA the NaChol partitioned both in SPC and TPA. The SPC–SPC homodimer as well as NaChol–Na+ adduct appeared after direct infusion of UDA in positive mode (Fig. 1Sc). The TPA and NaChol signals, the PGPMe–NaChol and the NaChol homodimer appeared after direct infusion of TPA:NaChol (6:1 w:w) organic solvent, negative mode (Fig. 1Sd). The TPA signals, the PGPMe–SPC heterodimer and the PGPMe–PGPMe homodimer, appeared after direct infusion of SPC:TPA (3:3 w:w) organic solvent, negative mode (Fig. 1Se). The signals of the SPC–SPC homodimer appeared in positive mode (Fig. 1Sf and d). Again the signals from infusion of mixtures in organic solvent suggested the hydrophobic effect was not underlying these non-covalent associations.

Overall, the non covalent interactions between NaChol and SPC as well as with TPA, were detected after direct infusion as heterodimers in the gas phase. These interactions are essential for NaChol partitioning within bilayers. The presence of SPC–PGPMe heterodimers indicated that in such proportions all components in UDA were soluble into each other, this fact accounting for the absence of microscopic domains. The PGPMe is the most abundant lipid in TPA, and contributes to maintain the stability of the archaea bilayer in hypersaline media [39]. The high volume of the PGPMe polar head is responsible for the membrane stabilization, causing steric repulsion between adjacent bilayers and avoiding aggregation [40]. Vesicles with a high content in PGPMe, form disordered phases made of separated non correlated bilayers, sponge like and opened that can not trap aqueous fluorescent markers such as carboxyfluorescein [40]. Such disordered lamellar phases [41] are due to repulsive forces derived from electrostatic repulsion between charged surfaces, out of plane ondulations of liquid crystalline flexible bilayers [42], or steric repulsion between bilayers containing voluminous headgroups. Together with the intermolecular non covalent associations between SPC–PGPMe and PGPMe–NaChol, the opened rich in PGPMe TPA bilayer would enable the fitting of SPC and NaChol, contributing to the absence of microscopic domains in UDL and UDA.

On the other hand, the impaired deformability caused by a difficult lateral NaChol displacement within TPA and reduced demixing in front of a mechanical stress, is strongly related to the high PGP–Me content of TPA. The lax, disordered more opened bilayers, with lower surface tension (small ΔH and large ΔS resulted in small ΔG) than those made of phospholipids [43] of PGP–Me, could be the reason for this phenomena. Paradoxically, although the chain-packing of PGPMe chains is less ordered in comparison with the crystalline phase–layer of the straight chain analogues, the rotational freedom of the phytanyl chains in these lipid–membranes ("lateral interdigitation") [44] as well as the segmental motion (*e.g.*, gauche–trans-gauche kink formation at the tertiary carbons), is restricted by the methyl side chains [45–47]. Moreover, the lateral diffusive motions of fluorescent dyes in branch-chained lipid membranes are lower than those for straight-chained lipid [45,48]. Additionally, the bulkier saccharide moiety of sugar archaeolipids such as SDGD-5 (the second majoritary component of TPA), may partly reduce the molecular motions, by establishing a hydrogen-bond network among headgroups. These arguments sustain the fact that the lipid molecular motions and in particular the lateral mobility of molecules capable of establishing hydrogen bondings with sugars, are probably reduced in TPA bilayers. This is compatible with a model of UDA where the SPC diluted sufficient enough the rich in PGPMe TPA bilayer, so as to the low lateral mobility of molecules (typical of rich in PGPMe bilayers) was no longer experienced.

3.3. Microscale morphology of GUVs

The use of giant unilamellar vesicles (GUVs) has proven to be a very valuable tool for the study of lipid–lipid and lipid–protein interactions [49–52]. Because of their size in the order of tens of micrometers, the GUVs can be observed in real time by a phase contrast microscope or an optical fluorescence microscope. Here we prepared GUVs by the electroformation method, and two different fluorescent lipid analogs were incorporated: FastDiO and DiIC18. FastDiO is an unsaturated lipid analog with a strong preference for disordered over ordered domains. DiIC18 is a saturated lipid analog that partitions more easily to ordered domains than FastDiO [53,54]. In this way, the microscale structural features of GUVs made of TPA:SPC:NaChol (3:3:1 w:w) and SPC:NaChol (6:1 w:w) (corresponding to highly deformable nanoliposomes) and of TPA:SPC:NaChol (4:2:1 w:w) (corresponding to non deformable nanoliposomes) were inspected by fluorescence confocal microscopy.

In Fig. S2 typical images of the products of electroformation obtained from the mixture SPC:NaChol (6:1 w:w) are shown. Both fluorescent lipid analogs homogenously partitioned in the GUVs (compare for instance Fig. S2a and b). No microscopic domains seemed to be present. The products of electroformation of this mixture included 0.6–0.7 μm thick tubules, both inside and outside the GUVs (see arrows in Fig. S2a and b). These bilayers moved noticeably as a result of thermal noise (see Fig. S2c) even during the few seconds it took to produce the images. This may indicate a high *D* or low Young's modulus of these GUVs.

In Fig. S3 typical images of the products of electroformation obtained from the mixture TPA:SPC:NaChol (3:3:1 w:w) are shown. The comparison of Fig. S3a with b and c showed that again, both fluorescent lipid analogs homogenously partitioned in the GUVs and no microscopic domains seemed to be present either. The products of electroformation included GUVs, many tubules both inside (see Fig. S3c) and outside the GUVs (approx. 0.2 μm thick) and a high amount of small vesicles, present mainly inside the GUVs (see arrows in Fig. S3b). In comparison with the GUV from SPC:NaChol (6:1 w:w), we observed a stronger tendency to produce vesicles of high curvature radii. In order to evaluate whether the TPA lipids had any influence in the formation of such of high curvature radii vesicles, GUVs with a higher amount of TPA were further prepared.

In Fig. 2 typical images of the products of electroformation obtained from the mixture TPA:SPC:NaChol (4:2:1 w:w) are shown. No signs of microscopic domains seemed to be present (FASTDiO images were not shown). The product of electroformation included a heterogeneous mixture of a few GUVs, 0.4–0.7 μm in diameter and 20–40 μm long tubules (see Fig. 2a), 1.2–2.3 μm diameter and 20–50 μm length membrane tubes, and a large amount of unilamellar vesicles both inside larger GUVs or organized as beads on a necklace. This last structure apparently was the result of the bilayer tubes being spontaneously invaginated until the membrane was fissioned in several sites, giving rise to many small vesicles one next to the other (see Fig. 2b and c). In agreement with recent observations by Šuštar and co-workers [55], it was observed that the trend to form vesicles of high curvature radii increased with the proportion of TPA in the GUV bilayers. Overall, the increase in the tubular forms (highly curved bilayer zones) and unilamellar vesicles together with the decrease in the number of GUV observed when compositions spanned from 3:3:1 to 4:2:1 (w:w) could arose from the increased content of PGPMe, a lipid with a voluminous headgroup exhibiting two negative charges. It is uncertain however if, besides to the impaired mobility, such morphology contributed to the lack of edge activator behavior of NaChol in TPA bilayers.

3.4. Penetration of protein loaded in different liposomal formulations

Most of the studies of skin penetration quantify the mass penetration as a function of depth without distinguishing between the histological features that are penetrated or diffused. Here, by exciting the autofluorescence of the skin at 405 nm and simultaneously exciting the fluorescence of the Alexa 647-labeled liposomal OVA at 633 nm, we observed that nanoliposomes could bring the macromolecule OVA across the SC to different depths of the viable epidermis. No fluorescence from free Alexa 647-labeled OVA was detected beyond the first micrometer of the SC (data not shown). We found a skin structure that was coincident with previous findings where pig and murine skin is described as structured into columns of cells separated by "canyons" of hydrophobic nature [56,57]. These canyons start as wrinkles in the surface and then close, giving rise to a structure that closely resembles the SC, and both in murine and in pig skin they traverse the whole epidermis reaching the Stratum Basale–Dermis plane. Such canyons have been suggested as the preferred path of penetration of liposomes applied to the skin [56,58]. The existence of clusters of cells separated by canyons where the liposomal material preferentially penetrated seems to be confirmed here for human skin, as shown in Fig. 3a–f. However, a more detailed study of human skin needs to be performed in order to ascertain that the structures observed here share the same properties as those observed in pig skin.

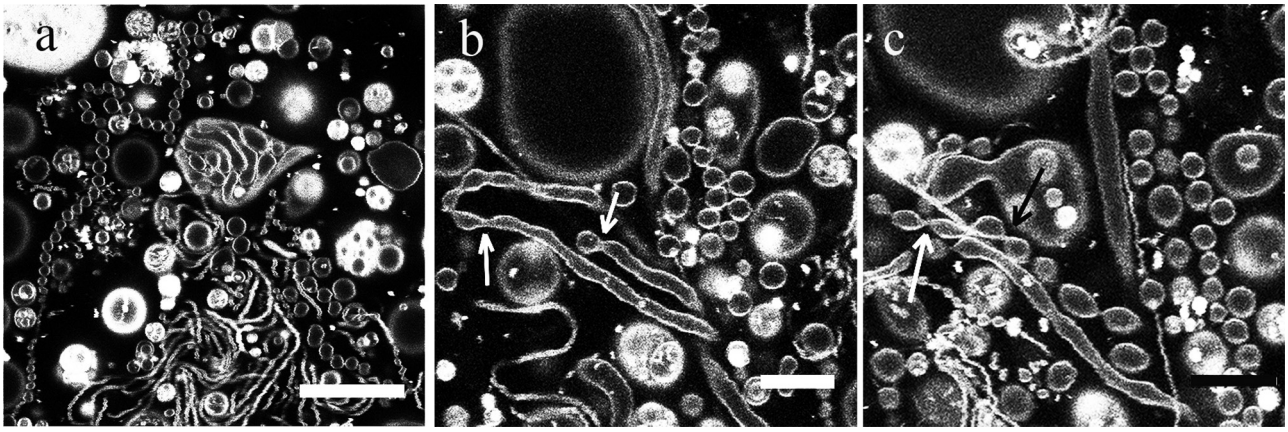

Fig. 2. Confocal fluorescence images of electroformation products from TPA:SPC:NaChol 4:2:1 w:w mixture. (a) A typical general view; (b) an image taken with larger magnification showing a membrane tube that is in the process of fission, the arrows mark the necks where the invagination is occurring; (c) an image taken a few seconds later in the same region as in (b), showing how the invagination of the membrane tube is almost complete (arrows). All images were taken in the DiI channel. Scale bars: 40 μm in a and 5 μm in (b) and (c).

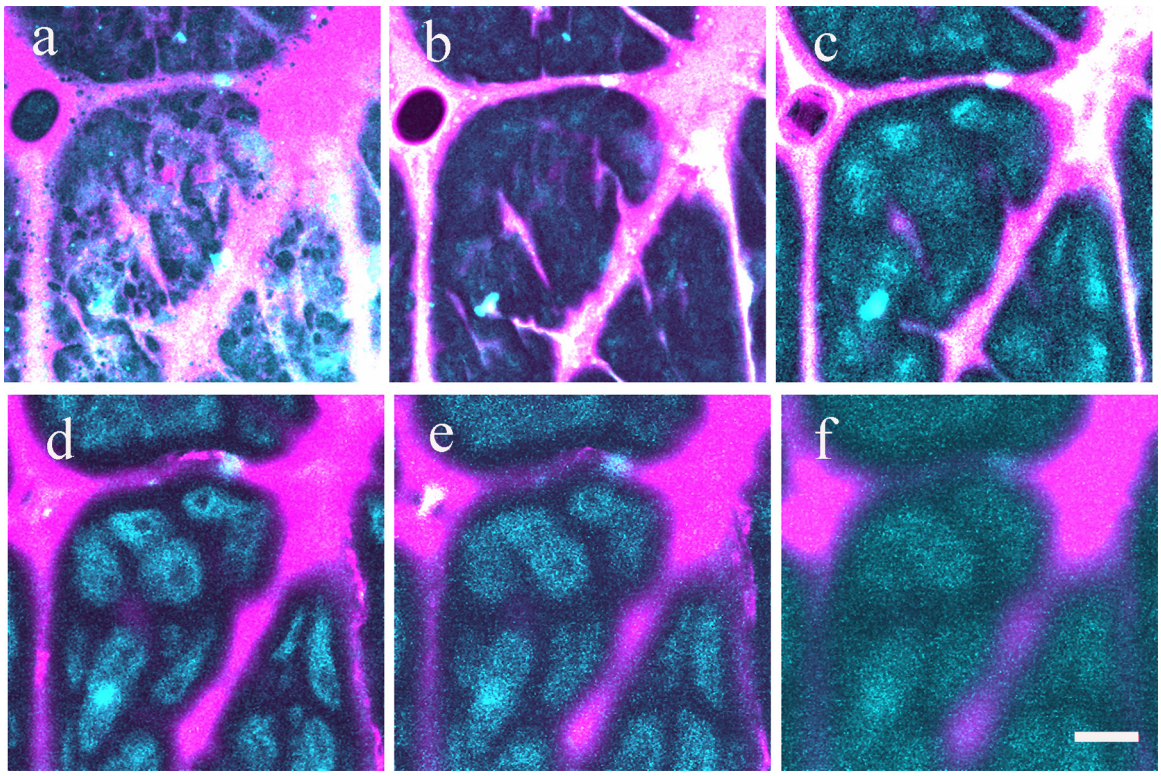

Fig. 3. Representative confocal fluorescence images of human skin, taken at different depths from the surface, incubated with Alexa 647 OVA–UDA. (a) at the surface; (b) at 10 μm from the surface; (c) at 30 μm; (d) at 50 μm; (e) at 65 μm; (f) at 80 μm from the surface. In cyan blue, skin autofluorescence. In magenta, fluorescence from Alexa 647 OVA. Scale bar: 100 μm.

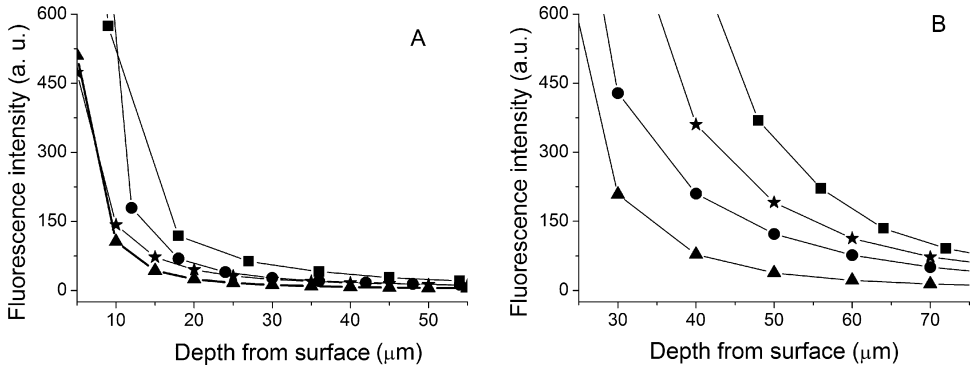

Fig. 4. Quantification of liposomal Alexa 647-OVA penetration in human skin. (a) penetration through cell clusters; (b) penetration through canyons. Squares, UDL; circles, L; triangles, ARC; stars, UDA. The error bars are of the same size as the symbols.

The areas corresponding to clusters and canyons of each micrograph were manually selected. The fluorescence intensity of each area of micrographs taken at different depth was determined according to Section 2. Next the intensities were plotted as a function of depth as shown, and divided in fluorescence in clusters and canyons for the four liposomal formulations. The fluorescence concentrated more in the canyons/wrinkles than in the cells clusters. As observed in Fig. 4a the fluorescence in clusters felt abruptly from high values at the surface, to zero at around 30 μm deep; the fluorescence in canyons shown in Fig. 4b persisted up to at least 90 μm. The trend in clusters and canyons nonetheless, was the same, reflecting the fact that the nanoliposomes entered OVA across the 50–100 μm wide canyons, to finally deliver it to the cell clusters. The UDL was the most efficient in entering OVA across canyons, followed by UDA, while the most inefficient formulation was ARC.

We observed that at 50 μm depth (nearly halfway the viable human skin epidermis (~50–100 μm according to the body site) [59,60], the fluorescence intensity in canyons decreased as follows: OVA–UDL > OVA–UDA> OVA-L> OVA–ARC. At such depth it is likely to find networks of Langerhans cells, typical antigen presenting cells of the epidermis, macrophages and in a much lower extent, immature dermal dendritic cells, potential targets of TPA containing liposomes [61,62]. Although UDA and UDL had no significant differences on *D* and Youngís modulus, UDL seemed more efficient than UDA in transporting OVA across the canyons, as judged by the fluorescence of nanoliposomal OVA in UDL, that was ~10 folds > ARC, ~3 folds > *L*, and ~1,5 folds > UDA. It can be speculated that the particulate (OVA ~ 7 nm hydrodynamic radii) material within nanoliposomes transported across the canyons, could suffer the steric hindrance caused by the voluminous structure of PGPMe in UDA bilayer (see Section 3). On the other hand, it is

important to point out that in this *in vitro* assay, most of the barrier properties of the epidermis remain intact between 2 and 6 months [63]. However, after a few weeks the cells are no longer viable, being thus unable of carrying out endocytic uptake [18]. Clearly for the endocytic uptake to take place, the material has first to access the cells across the canyons. But, since neither the liposomes not the OVA enter the cells by diffusion, but by energy dependent endocytic uptake [64], the fluorescence in cell clusters would not necessarily reflect the actual *in vivo* situation. Here the fluorescence in canyons suggested that the deformability was not straightly correlated to the penetration depth of nanoliposomal OVA.

4. Conclusions

Overall, our preliminary results suggested that the impaired deformability of nanoliposomes was owed to their high content of PGP–Me. This made difficult the lateral NaChol displacement within TPA, reducing the demixing in front of a mechanical stress. By quantifying the fluorescent OVA transported across the canyons, we found that *in vitro*, UDA were not optimally suited to efficiently transfer OVA across the human epidermis. To make profit of the immunological properties of TPA in liposomal mediated topical vaccination, further structural refinements will be required, for instance by replacing NaChol by a different edge activator. Different to SDGD5, PGPMe does not play an immunologic role. If PGPMe was the main responsible for the impaired lateral displacement of NaChol and the lower penetration of OVA in UDA, selectively increasing the SDGD5 content of UDA, could be another attractive alternative of choice.

Acknowledgments

This work was supported by CONICET PIP-2010-2012 893, EULANEST project Nanoskin and Secretaria de Investigaciones, Universidad Nacional de Quilmes. DCC, LHH, MJM and ELR are members of the Research Career Program from CONICET.

Appendix A. Supplementary data

Supplementary data associated with this article can be found, in the online version, at http://dx.doi.org/10.1016/j.colsurfb.2014.05.015.

References

[1] G. Cevc, G. Blume, Lipid vesicles penetrate into intact skin owing to the transdermal osmotic gradients and hydration force, Biochim. Biophys. Acta 1104 (1992) 226.
[2] P.L. Honeywell-Nguyen, G.S. Gooris, J.A. Bouwstra, Quantitative assessment of the transport of elastic and rigid vesicle components and a model drug from these vesicle formulations into human skin *in vivo*, J. Invest. Dermatol. 123 (2004) 902.
[3] J. Montanari, C. Maidana, M.I. Esteva, C. Salomon, M.J. Morilla, E.L. Romero, Sunlight triggered photodynamic ultradeformable liposomes against *Leishmania braziliensis* are also leishmanicidal in the dark, J. Controlled Release 147 (2010) 368.
[4] D. Mishra, V. Dubey, A. Asthana, D.K. Saraf, N.K. Jain, Elastic liposomes mediated transcutaneous immunization against hepatitis B, Vaccine 24 (2006) 4847.
[5] D. Mishra, P.K. Mishra, V. Dubey, M. Nahar, S. Dabadghao, N.K. Jain, Systemic and mucosal immune response induced by transcutaneous immunization using hepatitis B surface antigen-loaded modified liposomes, Eur. J. Pharm. Sci. 33 (2008) 424.
[6] D. Mishra, P.K. Mishra, S. Dabadghao, V. Dubey, M. Nahar, N.K. Jain, Comparative evaluation of hepatitis B surface antigen-loaded elastic liposomes and ethosomes for human dendritic cell uptake and immune response, Nanomedicine 6 (2010) 110.
[7] A. Corcelli, S. Lobasso, Methods in microbiology, in: F.A. Rainey, A. Oren (Eds.), Characterization of Lipids of Halophilic Archaea, 35, Elsevier, Amsterdam, 2006 (Chapter 25).
[8] L. Krishnan, C.J. Dicaire, G.B. Patel, G.D. Sprott, Archaeosome vaccine adjuvants induce strong humoral, cell-mediated, and memory responses: comparison to conventional liposomes and alum, Infect. Immnun. 68 (2000) 54.
[9] L.H. Higa, P. Schilrreff, A.P. Perez, M. Iriarte, D.I. Roncaglia, M.J. Morilla, E.L. Romero, Ultradeformable archaeosomes as new topical adjuvants, Nanomedicine 8 (2012) 1319.
[10] R.O. Gonzalez, L.H. Higa, R.A. Cutrullis, M. Bilen, I. Morelli, D.I. Roncaglia, R.S. Corral, M.J. Morilla, P.B. Petray, E.L. Romero, Archaeosomes made of *Halorubrum tebenquichense* total polar lipids: a new source of adjuvancy, BMC Biotechnol. 9 (2008) 71.
[11] M.K.S. Kates, in: E.M. DsaF (Ed.), Archaea. A Laboratory Manual, Cold Spring Harbor Laboratory, New York, NY, 1986 (Protocol 5, Isoprenoids and polar lipids of extreme halophiles. Halophiles).
[12] C.J.F. Bötcher, C.M. van Gent, C. Pries, A rapid and sensitive submicron phosphorus determination, Anal. Chim. Acta 24 (1961) 203.
[13] D.W. Fry, J.C. White, I.D. Goldman, Rapid separation of low molecular weight solutes from liposomes without dilution, Anal. Biochem. 90 (1978) 809.
[14] M.M. Bradford, A rapid and sensitive method for the quantitation of microgram quantities of protein utilizing the principle of protein-dye binding, Anal. Biochem. 72 (1976) 248.
[15] B.A. van den Bergh, P.W. Wertz, H.E. Junginger, J.A. Bouwstra, Elasticity of vesicles assessed by electron spin resonance, electron microscopy and extrusion measurements, Int. J. Pharm. 217 (2001) 13.
[16] M.I. Angelova, D. Dimitrov, Liposome electroformation, Faraday Discuss. Chem. Soc. 81 (1986) 303.
[17] A.-J. Garcia-Saez, D.C. Carrer, P. Schwille, Biological membrane models, methods in molecular biology, in: V. Weissig (Ed.), Liposomes: Methods and Protocols, vol. 2, Humana Press, Clifton, NJ, 2010 (Fluorescence correlation spectroscopy for the study of membrane dynamics and organization in giant unilamellar vesicles).
[18] X.H. Wang, J. Wu, N. Zhang, X.W. Chen, L.X. Zhou, G.X. Xiao, An experimental study on preservation of human split thickness skin samples with −20 °C non-freezing composite cryoprotective solution, Acta Acad. Med. Mil. Tertiae 24 (2002) 225.
[19] L.H. Higa, A.P. Perez, L. Arnal, C. Weissmann, O. Yantorno, M.E. Vela, M.J. Morilla, E.L. Romero, Topical immunization with ultradeformable archaeosomes carrying whole *Leishmania braziliensis* antigens, Int. J. Nanomed. (2014) (submitted).
[20] M. Guangzhao, X. Liang, K.Y. Simon Ng, Direct force measurement of liposomes by atomic force microscopy, in: Deker Encyclopedia of Nanoscience and Nanotechnology, Marcel Dekker Inc., New York, 2004, pp. 933.
[21] G. Cevc, Transfersomes, liposomes and other lipid suspensions on the skin: permeation enhancement, vesicle penetration, and transdermal drug delivery, Crit. Rev. Ther. Drug Carrier Syst. 13 (1996) 257.
[22] G. Cevc, A. Schatzlein, H. Richardson, U. Vierl, Overcoming semi-permeable barriers, such as the skin, with ultradeformable mixed lipid vesicles, transfersomes, liposomes or mixed lipid micelles, Langmuir 19 (2003) 10753.
[23] www. piercenet.com/products/sodium-IRcholate.
[24] G. Cevc, Material transport across permeability barriers by means of lipid vesicles, in: R. Lipowsky (Ed.), Handbook of Physics of Biological Systems, vol. I, Elsevier Science, Amsterdam, 1995 (Chapter 9).
[25] J.B. Fenn, M. Mann, C.K. Meng, S.F. Wong, C.M. Whitehouse, Electrospray ionization for mass spectrometry of large biomolecules, Science 246 (1989) 64.
[26] K. Yang, X. Han, Accurate quantification of lipid species by electrospray ionization mass spectrometry—meet a key challenge in lipidomics, Metabolites 1 (2011) 21.
[27] J. Berg, J. Tymoczko, L. Stryer, Biochemistry Series Michelle Julet, fifth ed., Freeman, New York, NY, 2002.
[28] J.A. Loo, Studying noncovalent protein complexes by electrospray ionization mass spectrometry, Mass Spectrom. Rev. 16 (1997) 1.
[29] J.M. Daniel, S.D. Friess, S. Rajagopalan, S. Wendt, R. Zenobi, Quantitative determination of noncovalent binding interactions using soft ionization mass spectrometry, Int. J. Mass Spectrom. 216 (2002) 1.
[30] G. Siuzdak, B. Bothner, Gas phase micelles, Angew. Int. Chem. Engl. 34 (1995) 18.
[31] N.T. Southall, K.A. Dill, A.D.J. Haymet, A view of the hydrophobic effect, J. Phys. Chem. B 106 (2002) 521.
[32] W. Kauzmann, Some factors in the interpretation of protein denaturation, Adv. Protein Chem. 14 (1959) 1.
[33] M. Sharon, L.L. Ilag, C.V. Robinson, Evidence for micellar structure in the gas phase, J. Am. Chem. Soc. 129 (2007) 8740.
[34] D.D. Lasic, On the thermodynamic stability of liposomes, J. Colloid Interface Sci. 140 (1990) 302.
[35] C. Bich, S. Baer, M.C. Jecklin, R. Zenobi, Probing the hydrophobic effect of noncovalent complexes by mass spectrometry, J. Am. Soc. Mass Spectrom. 21 (2010) 286.
[36] S.I. Simoesa, C.M. Marquesa, M.E.M. Cruza, G. Cevc, M.B.F. Martins, The effect of cholate on solubilisation and permeability of simple and protein-loaded phosphatidylcholine/sodium cholate mixed aggregates designed to mediate transdermal delivery of macromolecules, Eur. J. Pharm. Biopharm. 58 (2004) 509.
[37] K.M.G. Taylor, D.Q.M. Craig, Physical methods of study: differential scanning calorimetry, in: V. Torchilin, V. Weissing (Eds.), Liposomes: A Practical Approach, Oxford University Press, Oxford, 2003 (Chapter 3).
[38] S. Mabrey, J.M. Sturtevant, Investigation of phase transitions of lipids and lipid mixtures by high sensitivity differential scanning calorimetry, Proc. Nat. Acad. Sci. U.S.A. 73 (1976) 3862.
[39] M. Kates, Membrane lipids of extreme halophiles: biosynthesis, function and evolutionary significance, Experientia 49 (1993) 1027.

[40] B.G. Tenchov, R.C. MacDonald, D.P. Siegel, Cubic phases in phosphatidylcholine–cholesterol mixtures: cholesterol as membrane fusogen, Biophys. J. 91 (2006) 2508.
[41] R. Koynova, B. Tenchov, G. Rapp, Effect of PEG-lipid conjugates on the phase behavior of phosphatidylethanolamine dispersions, Colloids Surf., A: Physicochem. Eng. Aspects 149 (1999) 571.
[42] W. Helfrich, Steric interaction of fluid membranes in multi-layer systems, Z. Naturforsch. 33a (1978) 305.
[43] T. Kitano, T. Onoue, K. Yamauchi, Archaeal lipids forming a low energy-surface on air–water interface, Chem. Phys. Lipids 126 (2003) 225.
[44] O. Dannenmuller, K. Arakawa, T. Eguchi, K. Kakinuma, S. Blanc, A.M. Albrecht, M. Schmutz, Y. Nakatani, G. Ourisson, Membrane properties of archaeal macrocyclic diether phospholipids, Chemistry 6 (2000) 645.
[45] T. Baba, H. Minamikawa, M. Hato, T. Handa, Hydration and molecular motions in synthetic phytanyl-chained glycolipid vesicle membranes, Biophys. J. 81 (2001) 3377.
[46] U. Bakowsky, U. Rothe, E. Antonopoulos, T. Martini, L. Henkel, H.-J. Freisleben, Monomolecular organization of the main tetraether lipid from *Thermoplasma acidophilum* at the water-air interface, Chem. Phys. Lipids 105 (2003) 31.
[47] L.C. Stewart, M. Kates, I.H. Ekiel, I.C.P. Smith, Molecular order and dynamics of diphytanylglycerol phospholipids: a 2H and 31P-NMR study, Chem. Phys. Lipids 54 (1990) 115.
[48] T.K. Khan, P.L. Chong, Studies of archaebacterial bipolar tetraether liposomes by perylene fluorescence, Biophys. J. 78 (2000) 1390.
[49] L. Kalvodova, N. Kahya, P. Schwille, R. Ehehalt, P. Verkade, D. Drechsel, K. Simons, Lipids as modulators of proteolytic activity of BACE. Involvement of cholesterol, glycosphingolipids, and anionic phospholipids *in vitro*, J. Biol. Chem. 280 (2005) 36815.
[50] I. López-Montero, M. Vélez, P.F. Devaux, Surface tension induced by sphingomyelin to ceramide conversion in lipid membranes, Biochim. Biophys. Acta 1768 (2007) 553.
[51] K. Trajkovic, C. Hsu, S. Chiantia, L. Rajendran, D. Wenzel, F. Wieland, P. Schwille, B. Brügger, M. Simons, Ceramide triggers budding of exosome vesicles into multivesicular endosomes, Science 319 (2008) 1244.
[52] S.L. Veatch, S.L. Keller, Seeing spots: complex phase behaviour in simple membranes, Biochim. Biophys. Acta 1746 (2005) 172.
[53] J. Zhao, J. Wu, F.A. Heberle, T.T. Mills, P. Klawitter, G. Huang, G. Costanza, G.W. Feigenson, Phase studies of model biomembranes: complex behavior of DSPC/DOPC/cholesterol, Biochim. Biophys. Acta 1768 (2007) 2764.
[54] M. Fidorra, A. Garcia, J.H. Ipsen, S. Härtel, L.A. Bagatolli, Melting of individual lipid components in binary lipid mixtures studied by FTIR spectroscopy, DSC and Monte Carlo simulations, Biochim. Biophys. Acta (BBA)—Biomembr. 1788 (2009) 600.
[55] V. Šuštar, J. Zelko, P. Lopalco, S. Lobasso, A. Ota, N. Poklar Ulrih, A. Corcelli, V. Kralj-Iglič, Morphology, biophysical properties and protein-mediated fusion of archaeosomes, PLoS One 7 (2012) e39401.
[56] D.C. Carrer, C. Vermehren, L.A. Bagatolli, Pig skin structure and transdermal delivery of liposomes: a two photon microscopy study, J. Controlled Release 132 (2008) 12.
[57] A. Schaetzlein, G. Cevc, Non-uniform cellular packing oft he stratum corneum and permeability barrier function of intact skin: a high-resolution confocal scanning microscopy study using highly deformable vesicles (Transfersomes), Br. J. Dermatol. 138 (1998) 583.
[58] B. Baroli, Penetration of nanoparticles and nanomaterials in the skin: fiction or reality? J. Pharm. Sci. 99 (2010) 21.
[59] P.H. Lambert, P.E. Laurent, Intradermal vaccine delivery: will new delivery systems transform vaccine administration? Vaccine 26 (2008) 3197.
[60] B. Combadiere, B. Mahe, Particle-based vaccines for transcutaneous vaccination, Comp. Immunol. Microbiol. Infect. Dis. 31 (2008) 293.
[61] J.F. Nicolas, B. Guy, Intradermal epidermal and transcutaneous vaccination: from immunology to clinical practice, Expert Rev. Vaccines 7 (2008) 1201.
[62] L. East, C.M. Isacke, The mannose receptor family, Biochim. Biophys. Acta 1572 (2002) 364.
[63] L. Ge, Z. Huang, H. Wei, Skin graft preservation, in: M. Spears (Ed.), Skin Grafts—Indications, Applications and Current Research, Intech, Rijeka, Croatia, 2011 (Chapter 13).
[64] K. Un, K. Sakai-Kato, Y. Oshima, T. Kawanishi, H. Okuda, Intracellular trafficking mechanism, from intracellular uptake to extracellular efflux, for phospholipid/cholesterol liposomes, Biomaterials 33 (2012) 8131.